# Extension of Zero-Voltage-Switching Range in Dual Active Bridge Converter by Switched Auxiliary Inductance

Hayato Higa and Jun-ichi Itoh
Dept. of Energy and Environment Science Engineering
Nagaoka University of Technology
Nagaoka, Niigata, Japan
hhiga@stn.nagaokaut.ac.jp, Itoh@vos.nagaokaut.ac.jp

*Abstract*— **This paper proposes a novel Dual Active Bridge (DAB) converter, which has an auxiliary inductor and a bi-directional switch connected in parallel to a transformer in order to achieve zero voltage switching (ZVS) over a wide load range and a wide battery voltage variation. In the proposed converter, the equivalent magnetizing inductance is changed by switching the auxiliary inductance depending on the output power. In order to achieve ZVS at light load, the equivalent magnetizing current is increased by connecting the auxiliary inductance in parallel. At heavy load, the equivalent magnetizing current is reduced without connecting the auxiliary inductance because ZVS is achieved without any increment of the equivalent magnetizing current. In addition, the auxiliary inductance is switched without the occurrence of DC-offset of the auxiliary-inductor current. In the experimental results, the ZVS range is extended by 50% at most. In addition, the high efficiency in the wide load is achieved by the switched auxiliary inductance.**

***Keywords—Dual Active Bridge Converter; Zero Voltage Swtichng (ZVS); Magnetizing inductance***

## I. INTRODUCTION

Recently, energy storage systems have been actively installed to electric vehicles (EV) [1-3] and DC micro-grid systems [4-5]. A bi-directional isolated DC-DC converter is required in low voltage battery systems. Due to its flexibility, a dual active bridge (DAB) converter is generally employed as the bi-directional isolated DC-DC converter [6-8]. The DAB converter can obtain a high efficiency because zero voltage switching (ZVS) is achieved. ZVS not only reduces switching loss but also eliminates the voltage surge occurring at the hard switching operation due to the reserve recovery. Consequently, a low voltage rating Si-MOSFET can be applied at the low voltage side (under 100V). However, the ZVS range is limited due to the operation of the DAB converter over a wide load range and a wide battery voltage variation [9], which are usually the requirements in the energy storage system. Furthermore, the transformer current is increased due to the increment of negative instantaneous power with the voltage fluctuation [10].

In order to extend the ZVS range, the some modulation schemes have been presented [11-14]. Pulse Width Modulation (PWM) is employed by using the phase-shift control [11-12]. Nevertheless, it is not always possible to achieve ZVS for all switches over the wide voltage variation because the direction of the inductor current which discharges the junction capacitor cannot be controlled at the light load or the medium load. In addition, the pulse frequency modulation (PFM) is applied depending on operation conditions [13-14]. In [13], the switching frequency is adjusted in order to achieve the minimum loss from the loss calculation. In [14], the operation point at ZVS condition is kept by using PWM and PFM. Furthermore, the volume of the transformer is decided by the minimum switching frequency.

As a difference approach for extension of the ZVS range and reduction in the inductor current, the variable leakage inductance of the transformer has been proposed [15]. In this literature, the leakage inductance becomes small at heavy load. On the other hand, the leakage inductance becomes large at light load. References [16-17] show the DAB converter with the tap changing transformer using bi-directional switch. In these literatures, the turn ratio of transformer is changed by the bi-directional switch in order to accord the input voltage and the output voltage considering the turn ratio. However, the sequence at the changing leakage inductance is not considered. In addition, the switching devices used for the variable leakage inductance must withstand the half value of the main current. Besides, the coupling coefficient of the transformer $k_c$ is designed to be low in order to achieve the ZVS range in wide load range [18]. However, the converter efficiency at the heavy load decreases compared to that of the high coupling coefficient ($k_c \geq 0.99$) due to large magnetizing current.

In this paper, with the aiming for extending the ZVS range over the wide battery-voltage variation and maintaining the high converter efficiency over the wide load range, the DAB converter with a switched auxiliary inductance is proposed. In the proposed converter, the bi-directional switch and the auxiliary inductance are connected in parallel to the transformer. The original contribution in this paper is that the equivalent magnetizing inductance is changed by switching the auxiliary inductance depending on the output power and the voltage condition. In order to decide the switching sequence of the bi-directional switch, the current detection is not required because the switching timing of bi-directional switch is synchronized to the peak and bottom of the carrier. In addition, the reactive of the inductor current at low voltage (LV) side is also reduced by the auxiliary-inductor current. The heavy load efficiency does not decrease because the auxiliary inductance is not connected by the turn off of the bi-directional switch when ZVS can be achieved without the auxiliary-inductor current.

This paper is organized as follows; firstly, the circuit configuration and the operation mode of the switched auxiliary inductance are explained. Second, the switching sequence of the additional switch in order to switch the auxiliary inductance is introduced. Finally, the effectiveness of the switched auxiliary inductance is confirmed by the experiment at two voltage conditions.

## II. Proposed Dual Active Bridge Converter

### A. Circuit configulation

Fig. 1 shows the configuration of a DAB converter with the switched auxiliary inductance. Two H-bridge converters output square waveforms to a high frequency transformer. Transferred power is controlled by a phase difference between a high voltage (HV) side converter and a LV side converter. In the DAB converter at light load, the inductor current $i_{pr}$ becomes too low to satisfy the condition of ZVS in the HV side switches. The transferred power $P_{ZVS}$ that limits the ZVS range is calculated by (1) [19].

$$P_{ZVS} = \frac{V_{in} N V_{out}}{\omega L} \delta_{ZVS} \left( 1 - \frac{|\delta_{ZVS}|}{\pi} \right) \tag{1}$$

The phase-shift angle $\delta_{ZVS}$ is calculated at the condition of $NV_{out} \le V_{in}$ and the condition of $NV_{out} > V_{in}$, in (2) and (3) respectively [19].

$$\delta_{ZVS} = \frac{\pi}{2} \left\{ 1 - \frac{2L_m + L}{2L_m} \frac{NV_{out}}{V_{in}} + 4\beta f_{sw} T_d \right\} \tag{2}$$

$$\delta_{ZVS} = \frac{\pi}{2} \left\{ 1 - \frac{2L_m}{2L_m + L} \frac{V_{in}}{NV_{out}} + 4\alpha f_{sw} T_d \right\} \tag{3}$$

where $L_m$ is the equivalent magnetizing inductance, $\alpha$ and $\beta$ are the coefficients which are decided by the power flow, and $T_d$ is dead time. The coefficients are decided to be $\alpha$=1 $\beta$=-1 in the charge mode, whereas the coefficients are decided to be $\alpha$=-1 $\beta$=1 in the discharge mode.

Note that the parasitic capacitance is excluded in the calculation. The ZVS range is extended by the smaller auxiliary inductance $L_m$ as shown in (2), whereas the ZVS range is not extended by the smaller auxiliary inductance as shown in (3). Therefore, the turn ratio of the transformer N is designed in order to obtain the condition of $V_{in} > NV_{out}$.

Fig. 2 shows operation waveforms at light load with /without switching the auxiliary inductance. At light load where ZVS is not achieved by only the inductor current of the

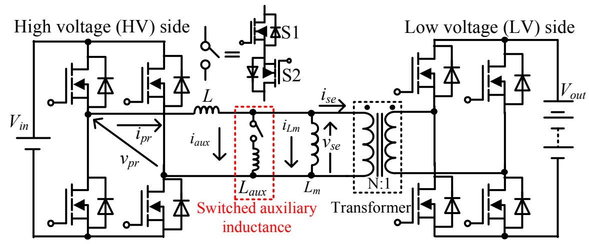


Fig. 1. Configuration of DAB converter with switched auxiliary inductance. When the additional switch is turned on at light load, ZVS is achieved by the auxiliary current. At the heavy load, the bi-directional switch is turned off in order to reduce the equivalent magnetizng current.

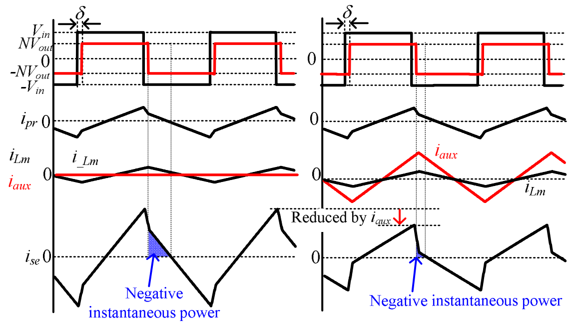


(a) Without switched $L_{aux}$. (b) With switched $L_{aux}$

Fig. 2. Operation waveforms of DAB converter with or without the switched auxiliary inductance. In order to achieve ZVS at light load, the auxiliary-inductor current is increased with the auxiliary inductor current. In the inductor current of LV side, the negative instantaneous power is reduced.

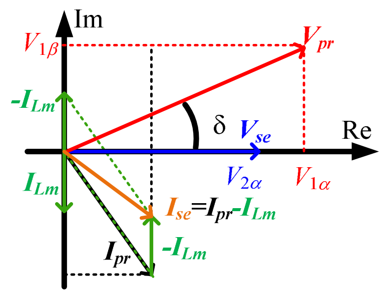


Fig. 3. Phaser diagram among voltages and the current in fundamental wave model of DAB converter. In Fig. 3, the reactive current is reduced by the equivalent magnetizng current $\boldsymbol{I_{Lm}}$.

HV side $i_{pr}$ and the LV side $i_{se}$, ZVS is achieved due to the auxiliary-inductor current when the auxiliary inductance is switched by turning on the bi-directional switch. At the heavy load, the bi-directional switch is turned off because ZVS can be achieved by only the inductor current at HV side and LV side. In Fig. 2 at the inductor current of the LV side, the negative instantaneous power is reduced. As a result, the reactive current of the inductor current at LV side is reduced by the auxiliary-inductor current. This reason is explained by using the sinusoidal wave model of the DAB converter with only the fundamental component of output voltage of each inverter $\boldsymbol{V_{pr}}$ and $\boldsymbol{V_{se}}$ [20].

Fig. 3 shows phaser diagram between the voltage and current of transformer [21]. In the sinusoidal model of the DAB converter, the output voltage of each inverter $\boldsymbol{V_{pr}}$, $\boldsymbol{V_{se}}$, are calculated by (4), (5) [20].

$$\boldsymbol{V_{pr}} = V_{1\alpha} + jV_{1\beta} \tag{4}$$

$$V_{se} = V_{2\alpha} \tag{5}$$

The inductor current of LV side $I_{se}$ with equivalent magnetizing inductance $L_m$ and the additional inductor $L$ is calculated by (6) [20].

$$I_{se} = I_{pr} - I_{Lm} = \frac{V_{1\beta}}{\omega L} + j\left\{\frac{V_{2\alpha} - V_{1\alpha}}{\omega L} - \left(-\frac{V_{2\alpha}}{\omega L_m}\right)\right\} \tag{6}$$

From (6), when the real part of primary voltage $V_{1\alpha}$ is larger than the real part of secondary voltage $V_{2\alpha}$, the reactive current of the inductor current at LV side is reduced by the auxiliary inductance $L_{aux}$ compared with only the magnetizing inductance $L_m$. In addition, the active current is not varied by the auxiliary-inductor current because only the reactive current is reduced by the auxiliary-inductor current.

## III. Switching Sequence of Additional Switch

Fig. 4 shows the relationship between the transient waveforms and the switching sequence of the additional switch to achieve the switched auxiliary inductance. Fig. 4(a) shows operation waveforms at the turn on of the additional switch, whereas Fig. 4(b) shows operation waveforms at the turn off of the additional switch. In the Fig. 4(a), the DC offset might occurs depending on the turn-on timing of bi-directional switch. In order to avoid this problem, the turn-on timing of S1 and S2 has to be set at the zero-crossing point of the magnetizing current $i_{Lm}$. Otherwise, the large inductor and the high current rating switch are required. In Fig. 4(b), the surge voltage occurs at the turn-off timing. The high voltage rating device is also required. In order to avoid the hard switching occurring in the bi-directional switch, the following switching sequence is proposed.

Fig. 5 shows the proposed switching sequence at switching

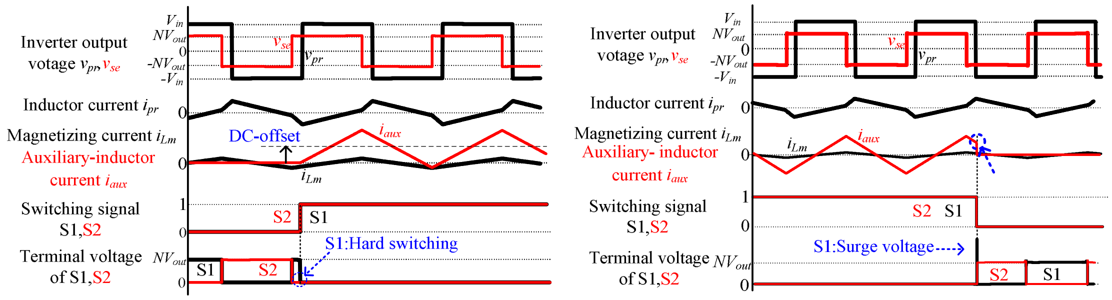


(a) Turn on of bi-directional switch (b) Turn off of bi-directional switch

Fig. 4. Operation waveforms of DAB converter with switched auxiliary inductance. At the turn-on of the bi-directional switch, the DC-offset might occur depending on the turn-on timing. At the turn-off of the bi-directional switch, the hard switching also occurs. As a result, the surge voltage occurs.

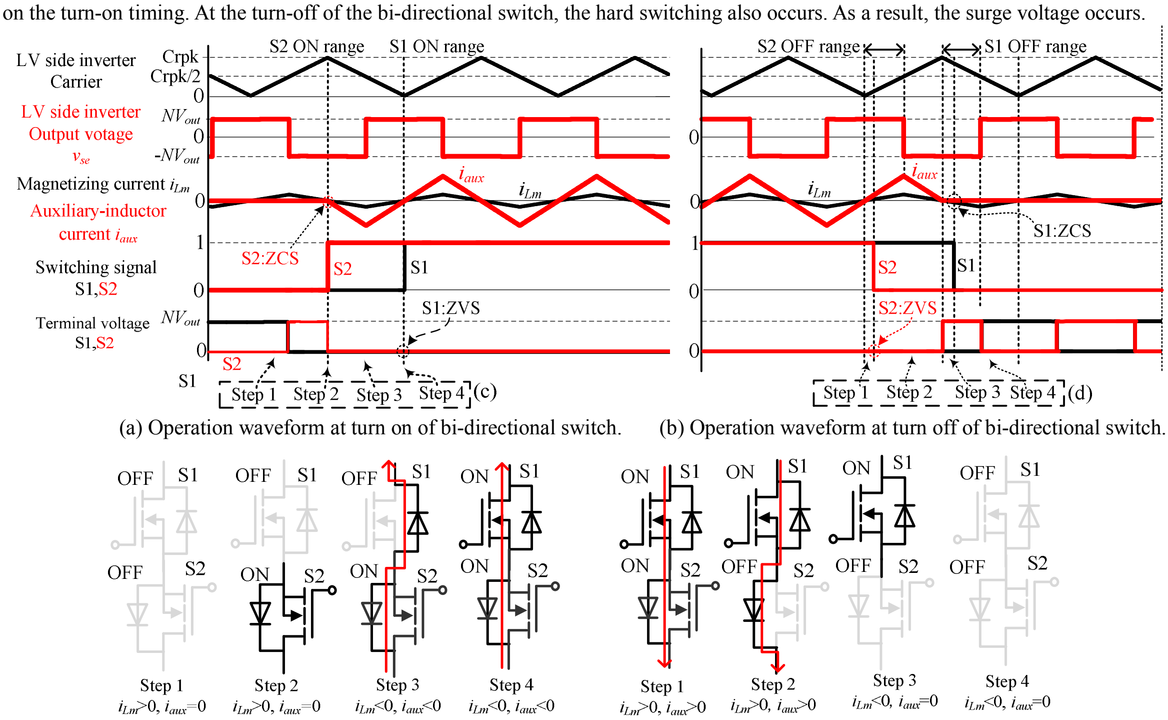


(a) Operation waveform at turn on of bi-directional switch. (b) Operation waveform at turn off of bi-directional switch.

(c) Turn-on of bi-directional switch (d) Turn-off of bi-directional switch

Fig. 5 Proposed switching sequence in order to switch auxiliary inductance. In the proposed switching sequence, the current detection is not required because the switching timing is synchronized to the carrier peak and bottom. The turn on of S1 or the turn off of S2 are ZVS because the body diode in S1 or S2 is turned on before the turn on of S1 or S2. Moreover, the DC-offset current does not occur. ZCS is achieved at the turn on of S2 and the turn off of S1, whereas ZVS is achieved at the turn off of S1. Hence, no surge voltage occurs at the turn off of S1 and S2.

the auxiliary inductance. Fig. 5(a) shows waveforms at the turn-on timing of the bi-directional switch, whereas Fig. 5(b) shows the waveforms at the turn-off timing of the bi-directional switch. In Fig. 5(a), there are four switching steps in order to turn on the bi-directional switch at the soft switching condition. First in step 1 of Fig. 5(a) and (c), S1 and S2 is off. Then in step 2, S2 is turned on at the point when the magnetizing current $i_{Lm}$ is zero cross, i.e. the point of the carrier peak. At the step 2, the turn on of S2 is the zero current switching (ZCS) operation because the auxiliary-inductor current $i_{aux}$ has not been flown yet. Then in step 3, the body diode of MOSFET in S1 is naturally turned on at $i_{Lm}$<0. Finally, S1 is turned on at the point when $i_{Lm}$ is zero cross point, i.e. the period of the carrier bottom. In addition, the DC offset does not occur because the turn-on timing of the body diode in MOSFET is zero cross point of the auxiliary current. In Fig. 5(b), there are also four switching steps in order to turn off the bi-directional switch at the soft switching condition. First in step 1 of Fig. 5(b) and (d), S1 and S2 are on. Then in step 2, S2 is turned off during the period when $i_{Lm}$ is positive, i.e. the period between the carrier bottom and half of the carrier peak. Note that at step 2, the auxiliary-inductor current $i_{aux}$ is not corrupted because of the commutation to the body diode in S2. Therefore, the turn off of S2 is ZVS. When $i_{Lm}$ becomes negative at step 3, the body diode in S2 is turned off naturally. Finally at step 4, S1 is turned off during the period when $i_{Lm}$ is negative, i.e. the period between the half of carrier peak and the carrier peak. Turn off of S2 and turn on of S1 are ZVS because the terminal voltage of S1 and S2 at the switching timing is zero. If the auxiliary inductance has to be inactive after the S1-off range, the switching timing order of S1 and S2 are switched. In the proposed switching sequence, the current detection is not required because switching timings of S1 and S2 are synchronized to the peak and bottom of the LV side carrier.

## IV. SIMULATION RESULTS

In this section, the simulation results are demonstrated in order to evaluate the effectiveness of the switched auxiliary inductance. Table I shows the simulation conditions. The auxiliary inductance $L_{aux}$ is 700 μH. It is noted that the transferred power which ZVS is achieved without the auxiliary inductance is 311 W from Eq. (1) and (2) in the discharge operation.

Fig. 6 shows the transient response of the switched auxiliary inductance at 173 W. Fig. 6(a) shows the transient response when turning on the bi-directional switch, i.e. the active of the switched auxiliary inductance. Fig. 6(b) shows the transient response at turning off the bi-directional switch, i.e. the inactive of the auxiliary inductance. In Fig. 6(a), the turn on of S2 is confirmed to be ZCS. In addition, the turn on of S1 is also ZVS At the turn on of bi-directional switch, the DC offset of the auxiliary-inductor current $i_{aux}$ does not occur. In Fig. 6(b), ZVS is achieved at the turn-off of S2. At the turn off of S1, ZCS is achieved. In the terminal voltages of S1 and S2, no surge voltage is confirmed. By using the switched auxiliary-inductor, the inductor current of the LV side is reduced by 43%.

Fig. 7 shows waveforms of the gate signal and drain-source voltage of the LV-side inverter at the condition of Fig. 6. Fig.

Table I Simulation condition

| | | | |
|---|---|---|---|
| Input voltage $V_{in}$ | 380 V | Additional inductor $L$ | 150 μH |
| Output voltage $V_{out}$ | 36 V | Rated power | 750 W |
| Switching frequency $f_{sw}$ | 100 kHz | Exciting inductance $L_m$ | 4 mH |
| Dead-time $T_d$ | 100 ns | Turn ratio of transformer $N$ | 8 |
| Auxiliary inductance | 700 μH | Battery voltage range | 36V to 60V |

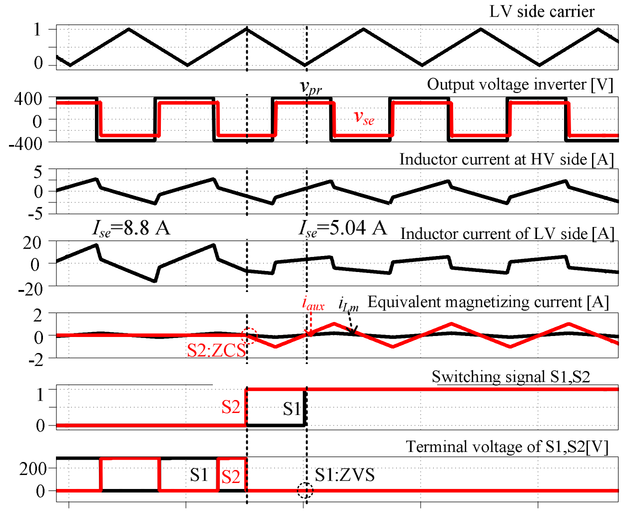


(a) Turn-on of bi-directional switch.

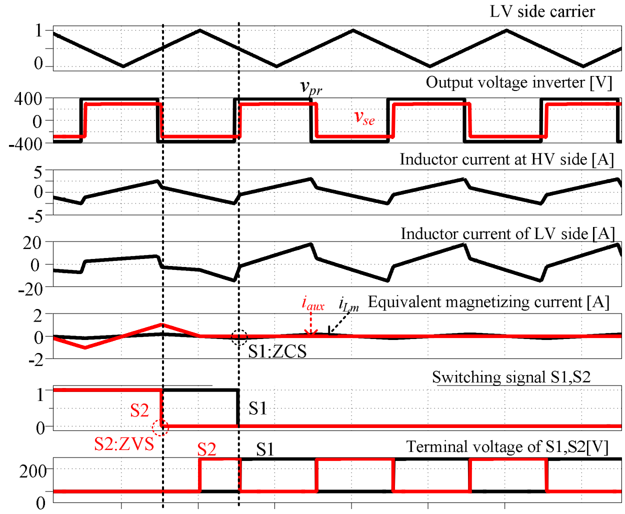


(b) Turn-off of bi-directional switch.

Fig. 6. Transient responses of switched auxiliary inductor in discharge operation at 173 W. At the switching timing of S1 and S2, ZVS or ZCS is achieved. Consequently, no surge voltage occurs. Furthermore, DC-offset does not occur in the auxiliary current

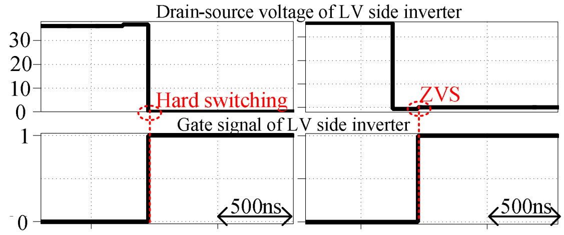


(a) Without switching $L_{aux}$ (b) With switching $L_{aux}$

Fig. 7. Waveforms of gate signal and drain-source voltage at 173 W. ZVS is achieved by the additional auxiliary current $i_{aux}$.

7(a) shows waveforms without the auxiliary inductance. Fig. 7(b) shows waveforms with switching the auxiliary inductance. In Fig. 7(b), ZVS is confirmed with the switched auxiliary inductance because MOSFET of the LV-side inverter are turned on at zero voltage.

Fig. 8 shows characteristics of the inductor current at LV side. In Fig. 8, the ZVS range with switching the auxiliary inductance is extended by 32% compared to that without switching the auxiliary inductance. Moreover, the inductor current of the LV side is reduced by 46.9% at most. However, the inductor current increases at the heavy load. Therefore, the light load efficiency can be improved by using the auxiliary inductance. Therefore, it is confirmed that the auxiliary inductance is changed according to the output power in order to achieve the high efficiency over the wide load range.

## V. EXPERIMENTAL RESULTS

In this section, experimental results are demonstrated in order to evaluate the switched auxiliary inductance in Table II. It is should be noted that the auxiliary inductor $L_{aux}$ and the additional inductor $L$ are connected to the primary side of the transformer. In the LV-side inverter of MOSFET, IRFP4110PbF (Infenion) is selected. IRFP4110PbF has the on-state resistance $R_{on}$ of 3.7 mΩ, the voltage rating $V_{rate}$ of 100 V and the current rating $I_{rate}$ of 120 A. On the other hand, SCT3030AL-E (Rohm) is selected at the HV-side inverter and the switched auxiliary inductor. SCT3030AL has the on-state resistance $R_{on}$ of 30 mΩ. In this paper, the diode clamp snubber circuit is used in order to reduce the resonant current between the auxiliary inductance and the parasitic capacitance of MOSFET (170 pF). The switching devices with low parasitic capacitance will be selected in the future work.

Fig. 9 shows operation waveforms with/without switching

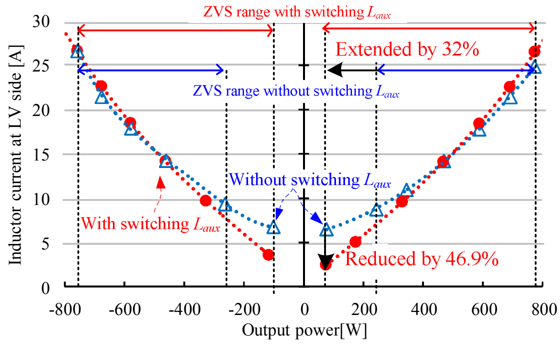


Fig. 8. Characteristic of inductor current with/without switched auxiliary inductance. The inductor current of LV side at the light load is reduced by 46.9% at most compared with the no switched auxiliary inductance.

Table II Experimental condition

| | | | |
|---|---|---|---|
| Input voltage $V_{in}$ | 190 V | Rated power | 220 W |
| Output voltage $V_{out}$ | 15, 18 V | Switching frequency $f_{sw}$ | 100 kHz |
| Dead-time at HV side | 100 ns | Turn ratio of transformer $N$ | $N_1/N_2$=24/3 |
| Dead-time at LV side | 150 ns | Auxillary inductance $L_{aux}$ | 700 μH |
| Additional inductor $L$ | 148 μH | Magnetizing inductance $L_m$ | 4.1mH |
| Inductor core shape PC40EI50-Z(TDK) | | Transformer core shape PC40 EI70×55×19(TDK) | |
| Auxiliary inductor core shape EE65-32-27(EPCOS) | | | |

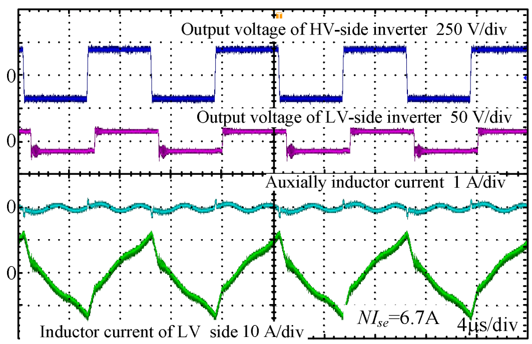


(a) $P_{out}$=65.1 W, without switching $L_{aux}$

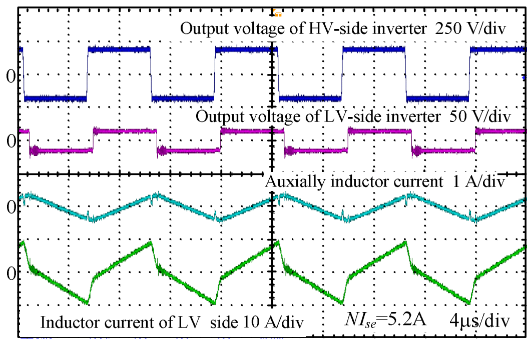


(b) $P_{out}$=70.4 W, with switching $L_{aux}$

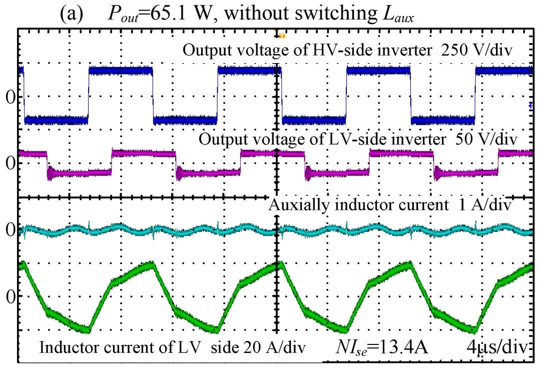


(c) $P_{out}$=168 W, without switching $L_{aux}$

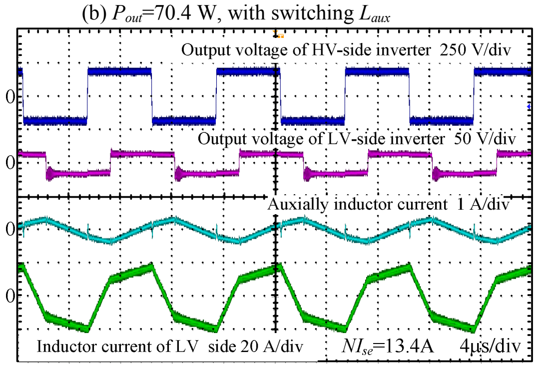


(d) $P_{out}$=164 W, with switching $L_{aux}$

Fig. 9. Operation waveforms with/without switching the auxiliary inductance when input voltage is 190 V, output voltage is 15 V. At light load as shown in (a) and (b), the inductor current in (b) is reduced by the increment of the equivalent magnetizing current. At heavy load as shown in (c) and (d), the inductor current is almost same because the real part of the HV side voltage is close to that of the LV side voltage.

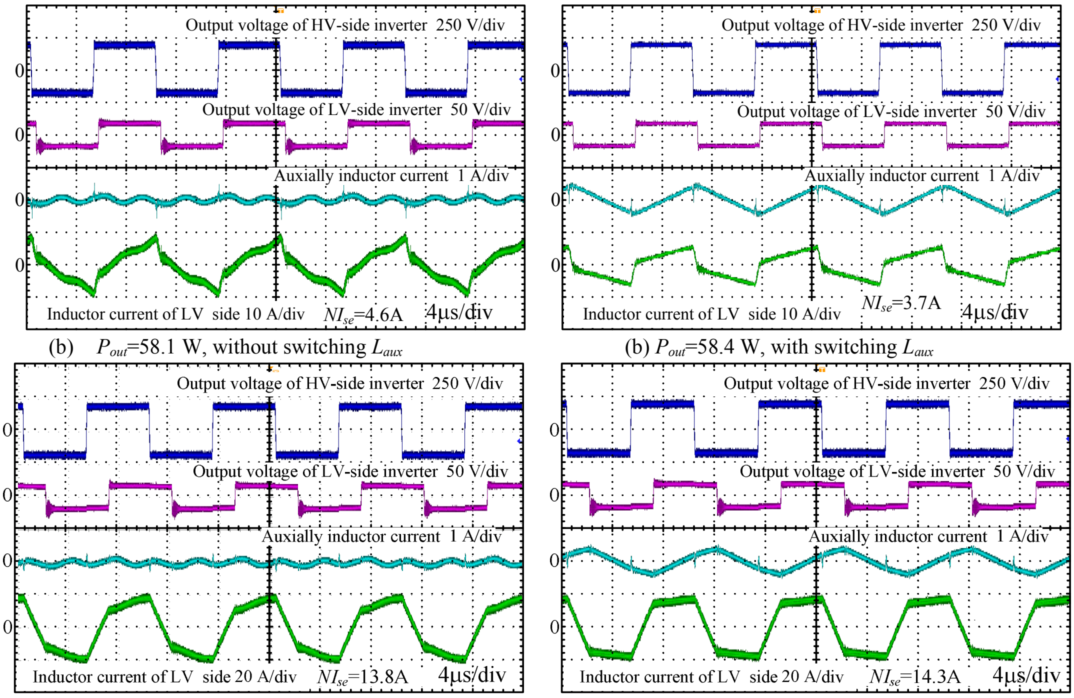


(b) $P_{out}$=58.1 W, without switching $L_{aux}$

(b) $P_{out}$=58.4 W, with switching $L_{aux}$

(c) $P_{out}$=200 W, without switching $L_{aux}$

(d) $P_{out}$=194 W, with switching $L_{aux}$

Fig. 10. Operation waveforms with/without switching auxiliary inductance when input voltage is 190 V, output voltage are 18 V. At light load as shown (a) and (b), the inductor current in (b) can still be reduced by the increment of the equivalent magnetizing current even at the different output voltage of 18V compared to Fig. 9.

the auxiliary inductor at the input voltage of 190 V, the output voltage of 15 V. The voltage ratio $NV_{out}/V_{in}$ is 0.63. Fig. 9(a) and (b) show operation waveforms at the light load with/without switching the auxiliary inductor. When the switched auxiliary inductance is active, the inductor current is reduced by the increment of the equivalent magnetizing inductance. In the inactive of the switched auxiliary inductor, the resonance between the auxiliary inductance $L_{aux}$ and the parasitic capacitance of the MOSFET $C_{ds}$ occurs. Besides, the output power is slightly different with/without switching the auxiliary inductance because the dead time error [22-23] occurs when the switching timing of the LV side inverter is close to zero cross point of the inductor current at the LV side in the condition of Fig. 9(b). Fig. 9(c) and (d) show operation waveforms at heavy load with/without switching the auxiliary inductor. Although the reactive current is reduced by the switching the auxiliary inductance, the inductor current is almost same as shown in Fig 9(c) and (d). This is because the real part of the LV side voltage $V_{2\alpha}$ is close to that of the HV side voltage $V_{1\alpha}$. Therefore, only the light load efficiency can be improved by the increment of equivalent magnetizing current.

Fig. 10 shows operation waveforms with/without switching the auxiliary inductor at the input voltage of 190 V, the output voltage of 18 V. The voltage ratio $NV_{out}/V_{in}$ is 0.76. Fig. 10(a) and (b) show operation waveforms at the light load with and without the auxiliary inductor. The inductor current of the LV side is reduced by 19%. When the auxiliary inductance is switched, ZVS can be achieved because the direction of the inductor current is adjusted in order to discharge the drain-source capacitance due to the switching of the auxiliary inductor. However, the inductor current at the heavy load is increased by the auxiliary inductor current as shown in Fig 10(c) and (d). This is because the real part of the LV side voltage $V_{2\alpha}$ is larger than the real part of the HV side voltage $V_{1\alpha}$ from (6). As a conclusion, the converter efficiency is improved by switching the auxiliary inductance depending on the voltage ratio and the output power.

Fig. 11 shows the transient response of the switching auxiliary inductance. At the turn on of bi-directional switch, it is confirmed that the DC offset of the auxiliary-inductor current $i_{aux}$ does not occur.

Fig. 12 shows operation waveforms of the gate signal and the drain-source voltage with/without switching the auxiliary inductance. In Fig. 12(a), the occurrence of the hard switching is confirmed, i.e. the turn on of MOSFET at the output voltage. The surge voltage occurs due to the reverse recovery current of body diode in MOSFET. In Fig. 10(b), ZVS is confirmed because MOSFET is turned on at zero voltage. In addition, the recover surge does not occur compared without the switching the auxiliary inductance.

Fig. 13 shows characteristics of the inductor current at the LV side with or without the auxiliary inductance. Fig. 13 (a) shows the inductor current of the LV side at the input voltage of 190 V and the output voltage of 15 V. In Fig. 13(a), the inductor current of the LV side with the auxiliary-inductor current is reduced by 25% at most compared with that of no auxiliary-inductor current. Fig. 13(b) shows the inductor current of the LV side at the input voltage of 190 V and the output voltage of 18 V. In Fig. 13(b), the inductor current of

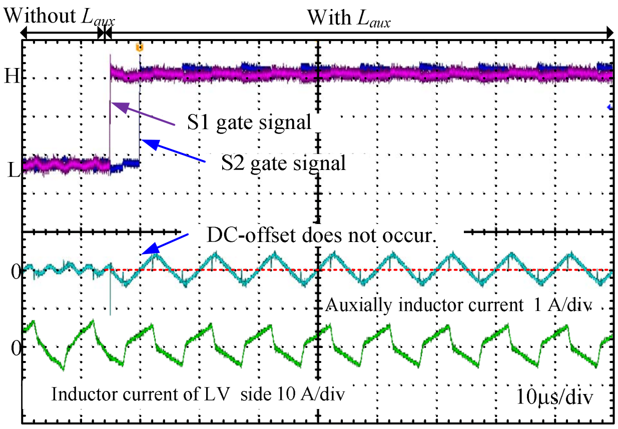


Fig. 11. Transient response of switched auxiliary inductance in discharge operation. By using the proposed switching sequence, DC-offset does not occur in the auxiliary current

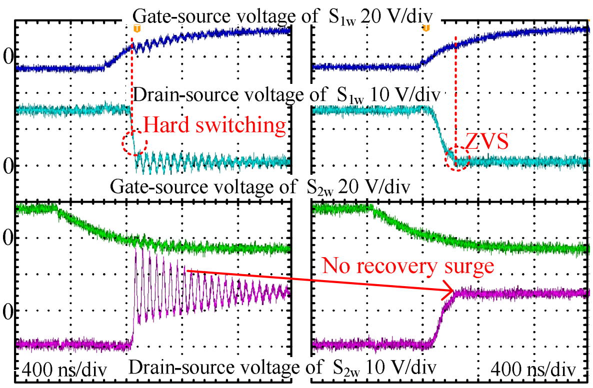


(a) Without switching $L_{aux}$ (b) With switching $L_{aux}$

Fig. 12. Waveforms of gate signal and drain-source voltage at light load. ZVS is not achieved without the auxiliary inductance, whereas ZVS is achieved by the switched auxiliary inductance. Therefore, the recovery surge is reduced by ZVS.

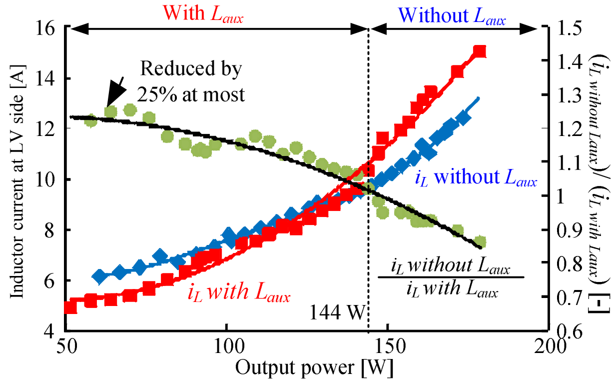


(a) $V_{in}$=190 V, $V_{out}$= 15 V

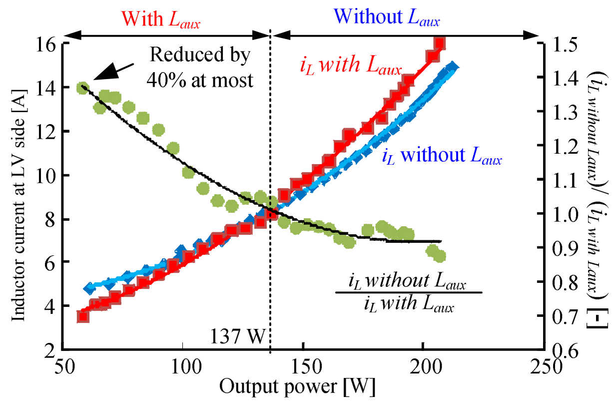


(b) $V_{in}$=190 V, $V_{out}$= 18V

Fig. 13. Characteristic of inductor current with/without switched auxiliary inductance. With the auxiliary inductance $L_{aux}$, the inductor current of LV side at the light load is reduced by 40% at most compared to the no switched auxiliary inductance. In Fig. (a) and (b), The changing point between two operation mode are 144 W and 137 W.

the LV side with the auxiliary-inductor current is also reduced by 28% at most compared with that of no auxiliary inductor. At heavy load with the auxiliary inductance, the inductor current is increased compared to that of the auxiliary inductance.

Fig. 14 shows the efficiency characteristics with/without the auxiliary inductance. Fig. 14(a) shows the efficiency characteristics at the input voltage of 190 V, the output voltage of 15 V, whereas Fig. 14(b) shows the efficiency characteristics at the input voltage of 190 V, the output voltage of 18 V. The maximum efficiencies in two voltage conditions are 95.9% and 95.4% when switching the auxliary inductance. By applying the switched auxilary inductance, the converter loss is reduced at light load region. At heavy load, the converter efficiency with $L_{aux}$ is decreased compared to that without $L_{aux}$ because the inductor current is increased by the incremnet of the auxiliary-inductor current. In Fig 14(a), the converter loss is reduced by 18% at most, whereas the ZVS range is extended by 50%. In Fig. 14(b), the converter loss is reduced by 21% at most compared without swithing the auxiliary inductance. Moreover, the ZVS range is extended by 29.2%. In Fig. 14(a) and (b), There are the changing points between two operation modes of 129 W and 110 W. In the proposed method, the high efficiency in wide load is achieved when the auxiliary-inductor is switched at the changing point. From above results that, the converter efficiency is impoved by the switching auxiliary inductance depending on the output power and the voltage condition.

## VI. Conclusion

This paper proposed the switching auxiliary inductor for the DAB converter in order to reduce the reactive current of the inductor current at the LV side and extend the ZVS range. In the proposed method, the equivalent magnetizing current is changed by switching the auxiliary-inductor depending on the output power. The switching sequence of the switched auxiliary inductor was also introduced in order to reduce the DC-offset current.

In the experiment, the operation with/without the switched auxiliary inductor was confirmed. Two maximum efficiencies of 95.4% and 95.9% at different output voltages of 15V and 18V were achieved by the switched auxiliary inductor. In addition, the converter loss was reduced by 21% at most by changing the equivalent magnetizing current. Moreover, the inductor current of the LV side was also reduced by 40%, whereas the ZVS range was extended by 50%. In the proposed switching sequence, the transient response without DC-offset current the auxiliary inductor was also confirmed.

In future work, the converter efficiency will be improved by the optimizing design of the auxiliary inductance and the additional inductor.

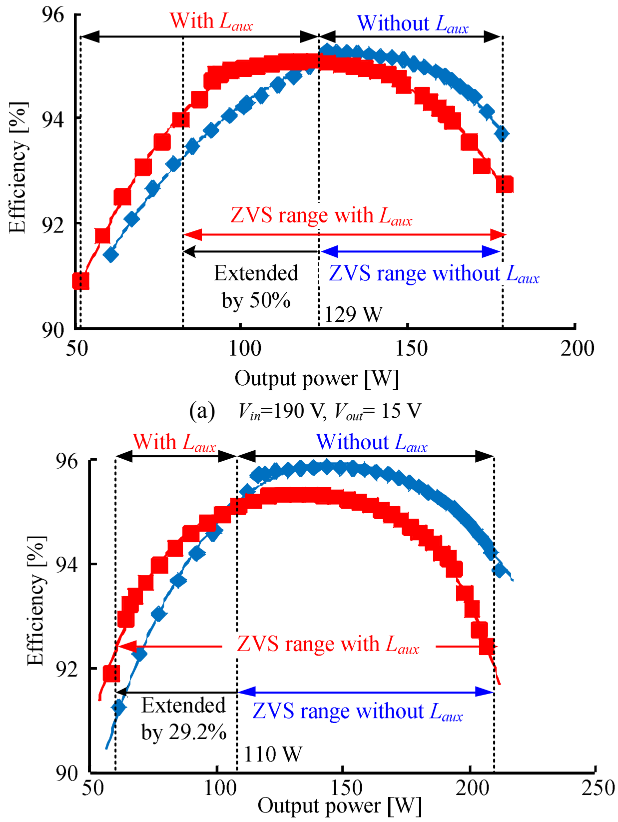


(a) $V_{in}$=190 V, $V_{out}$= 15 V

(b) $V_{in}$=190 V, $V_{out}$= 18 V

Fig. 14 Efficiency characteristics of prototype with switched auxiliary inductor. At the light load, the converter loss is reduced by 38.3% at most when the switched auxiliary inductor is active. In addition, the ZVS range is extended by 50% at most. In Fig. (a) and (b), The changing points between two operation modes are 129 W and 110 W. Therefore, the high efficiency in wide load is achieved when the auxiliary-inductor is switched at the changing point.

## REFERENCES


[1] Florian Krismer, Johann W. Kolar: "Efficiency-Optimized High-Current Dual Active Bridge Converter for Automotive Applications", IEEE Trans. IE., Vol. 59, No. 7, pp. 2745-2760 (2012)

[2] Pham Xuan Khiet; Yasunori Mitani; Masayuki Watanabe; Hisafumi Yamada; Yaser Solimar Qudaih; Kiyotaka Fuji "Development and evaluation of DC-DC converter for isolated PV power supply system with EV" International Power & Energy Conference (IPEC), pp. 424 – 427 (2012)

[3] Du, Yu ; Lukic, Srdjan ; Jacobson, Boris ; Huang, Alex : "Review of high power isolated bi-directional DC-DC converters for PHEV/EV DC charging infrastructure", Energy Conversion Congress and Exposition (ECCE) 2011, pp.553-560, (2011)

[4] Luis M. Miranda, Diogo Varajão, Bruno dos Santos, Rui E. Araújo: "Power flow control with bidirectional dual active bridge battery charger in low-voltage microgrids", EPE2013 (2013)

[5] M. Mao, Zheng Dong; Yong Ding, Liuchen Chang "Accurate Output Power Control of Converters for Microgrids Based on Local Measurement and Unified Control", IEEJ Journal of Industry Applications, Vol. 4, No. 4, pp.331-338, 2015.

[6] Rik W.A. De Donker, Deepakaraj M. Divan, Mustansir H Kheraluwala: "A Three-Phase Soft Switched High-Power-Density dc/dc Converter for High-Power Applications ", IEEE Trans. IAS, Vol. 27, No. 1, pp. 63-73 (1991)

[7] Hirofumi Akagi, Tatsuya Yamagishi, Nadia Mei Lin Tan, Shin-ichi Kinouchi, Yuji Miyazaki, Masato Koyama: "Power-Loss Breakdown of a 750-V 100-kW 20-kHz Bidirectional Isolated DC–DC Converter Using SiC-MOSFET/SBD Dual Modules", IEEE Trans.IAS., Vol. 51, No. 1, pp. 420-428 (2015)

[8] Florian Krismer, Johann W. Kolar: "Efficiency-Optimized High-Current Dual Active Bridge Converter for Automotive Applications", IEEE Trans. IE., Vol. 59, No. 7, pp. 2745-2760 (2012)

[9] A. Jones, B. Smith, C. Maxwell: "Reactive Power Loss Optimization Method for Bi-directional Isolated DC-DC Converters", IPEC-Hiroshima2014, pp. 702-706 (2014)

[10] Florian Krismer, Johann W. Kolar: "Accurate Power Loss Model Derivation of a High-Current Dual Active Bridge Converter for an Automotive Application", IEEE Trans. IE., Vol. 57, No. 3, pp. 881-891 (2010)

[11] A. K. Jain, R. Ayyanar: "PWM Control of Dual Active Bridge: Comprehensive Analysis and Experimental Verification", IEEE Trans on Power Electronics, Vol, 26, No. 4, pp. 1215-1227, 2011.

[12] Florian Krismer, Johann W. Kolar: "Closed Form Solution for Minimum C+onduction Loss Modulation of DAB Converters", IEEE Trans. PELS., Vol. 27, No. 1, pp. 174-188 (2012)

[13] Felix J. and Jurgen B., "Generalized Modeling and Optimization of a Bidirectional Dual Active Bridge DC-DC Converter Including Frequency Variation", IEEJ Journal of Industry Applications, Vol.4, No.5, pp.593-601, 2015.

[14] Giuseppe Guidi, Atsuo Kawamura, Yuji Sasaki, Tomofumi Imakubo: "Dual Active Bridge Modulation with Complete Zero Voltage Switching Taking Resonant Transitions into Account", EPE2011, pp.1-10 (2011)

[15] G. Guidi, M. Pavlovsky, A. Kawamura, T. Imakubo, Y. Sasaki: "Improvement of Light Load Efficiency of Dual Active Bridge DC-DC Converter by Using Dual Leakage Transformer and Variable Frequency", ECCE2010, pp. 830-837 (2010)

[16] Silvano Taraborrelli, Ren`e Spenke, Rik W. De Doncker: "Bidirectional DC-DC Converter based on a Dual Active Bridge with Tap Changer", EPE2016, (2016)

[17] S. M. Shiva et al., "Tap changing transformer based dual active bridgebi-directional DC-DC converter," ICPE-ECCE Asia 2015, pp. 2025-2030.(2017)

[18] J. Riedel, D.G. Holmes, C. Teixeira, B.P. McGrath: "Wide Range ZVS Operation of Dual Active Bridge DC-DC Converter using Adaptive Modulation and Low Coupling Factor Transformers", EPE2016, 2016.

[19] M.N., Gascoigne, R.W., Divan, D.M., Baumann, E.D.: "Performance Characterization of a High Power Dual Active Bridge dc-to-dc Converter", IEEE Trans. IA., Vol. 28, No. 6, pp. 1294-1301, (1992).

[20] J. Itoh, H. Higa, T. Nagano: "A Novel Control Method Focusing on Reactive Power for a Dual Active Bridge Converter ", IEEE International Power Electronics and Application Conference and Exposition, TS.8.34.1, (2014).

[21] Shun Nagata, Mika Takasaki, Yutaka Furukawa, Toshiro Hirose, Yoichi Ishizuka: "A Static Characteristic Analysis of Proposed Bi-Directional Dual Active Bridge DC-DC Converter", IPEC-Hiroshima2014, pp. 2252 −2259 (2014)

[22] Biao Zhao, Qiang Song, Wenhua Liu, Yandong Sun: "Dead-Time Effect of the High-Frequency Isolated Bidirectional Full-Bridge DC - DC Converter:Comprehensive Theoretical Analysis and Experimental Verification", IEEE Trans. PELS., Vol. 29, No. 4, pp. 1667-1680, (2014)

[23] Kazuto Takagi, Hideaki Fujita: "Dynamic Control and Dead-Time Compensation Method of an Isolated Dual-Active-Bridge DC-DC Converter", EPE2015, (2015)